Stochastic multi-scale prediction on the apparent elastic moduli of trabecular bone considering uncertainties of biological apatite (BAp) crystallite orientation and image-based mo...

Article *in* Computer Methods in Biomechanics and Biomedical Engineering · April 2013

DOI: 10.1080/10255842.2013.785537 · Source: PubMed

CITATIONS
18

READS
135

3 authors:

Khairul Salleh Basaruddin
Universiti Malaysia Perlis
116 PUBLICATIONS **265** CITATIONS
SEE PROFILE

Naoki Takano
Keio University
199 PUBLICATIONS **1,318** CITATIONS
SEE PROFILE

Takayoshi Nakano
Osaka University
590 PUBLICATIONS **8,098** CITATIONS
SEE PROFILE

Computer Methods in Biomechanics and Biomedical Engineering

Publication details, including instructions for authors and subscription information:
http://www.tandfonline.com/loi/gcmb20

Stochastic multi-scale prediction on the apparent elastic moduli of trabecular bone considering uncertainties of biological apatite (BAp) crystallite orientation and image-based modelling

Khairul Salleh Basaruddin [a d], Naoki Takano [b] & Takayoshi Nakano [c]

[a] Graduate School of Science and Technology, Keio University, 3-14-1 Hiyoshi, Yokohama, 223-8522, Japan

[b] Department of Mechanical Engineering, Keio University, 3-14-1 Hiyoshi, Yokohama, 223-8522, Japan

[c] Division of Materials and Manufacturing Science, Osaka University, 2-1 Yamadaoka, Suita, Osaka, 565-0871, Japan

[d] School of Mechatronic Engineering, Universiti Malaysia Perlis, 02600 Ulu Pauh, Perlis, Malaysia

Version of record first published: 14 Apr 2013.

To cite this article: Khairul Salleh Basaruddin , Naoki Takano & Takayoshi Nakano (2013): Stochastic multi-scale prediction on the apparent elastic moduli of trabecular bone considering uncertainties of biological apatite (BAp) crystallite orientation and image-based modelling, Computer Methods in Biomechanics and Biomedical Engineering, DOI:10.1080/10255842.2013.785537

To link to this article: http://dx.doi.org/10.1080/10255842.2013.785537

Computer Methods in Biomechanics and Biomedical Engineering, 2013
http://dx.doi.org/10.1080/10255842.2013.785537

Stochastic multi-scale prediction on the apparent elastic moduli of trabecular bone considering uncertainties of biological apatite (BAp) crystallite orientation and image-based modelling

Khairul Salleh Basaruddin[a,d]*, Naoki Takano[b] and Takayoshi Nakano[c]

[a]*Graduate School of Science and Technology, Keio University, 3-14-1 Hiyoshi, Yokohama 223-8522, Japan;* [b]*Department of Mechanical Engineering, Keio University, 3-14-1 Hiyoshi, Yokohama 223-8522, Japan;* [c]*Division of Materials and Manufacturing Science, Osaka University, 2-1 Yamadaoka, Suita, Osaka 565-0871, Japan;* [d]*School of Mechatronic Engineering, Universiti Malaysia Perlis, 02600 Ulu Pauh, Perlis, Malaysia*

(*Received 24 November 2012; final version received 11 March 2013*)

An assessment of the mechanical properties of trabecular bone is important in determining the fracture risk of human bones. Many uncertainty factors contribute to the dispersion of the estimated mechanical properties of trabecular bone. This study was undertaken in order to propose a computational scheme that will be able to predict the effective apparent elastic moduli of trabecular bone considering the uncertainties that are primarily caused by image-based modelling and trabecular stiffness orientation. The effect of image-based modelling which focused on the connectivity was also investigated. A stochastic multi-scale method using a first-order perturbation-based and asymptotic homogenisation theory was applied to formulate the stochastically apparent elastic properties of trabecular bone. The effective apparent elastic modulus was predicted with the introduction of a coefficient factor to represent the variation of bone characteristics due to inter-individual differences. The mean value of the predicted effective apparent Young's modulus in principal axis was found at approximately 460 MPa for respective 15.24% of bone volume fraction, and this is in good agreement with other experimental results. The proposed method may provide a reference for the reliable evaluation of the prediction of the apparent elastic properties of trabecular bone.

Keywords: trabecular bone; uncertainties; apparent elastic moduli; image-based modelling; stochastic multi-scale analysis

1. Introduction

An assessment of the mechanical properties of trabecular bone is essential when the 'bone quality' becomes a matter of concern in order to examine the fracture risk of human bones. The apparent mechanical properties of trabecular bone rely on many factors. In the context of bone characteristics, the effect of variations of bone volume fraction (Carter and Hayes 1977; Keyak et al. 1994), micro-architecture (Dempster 2000; Pothuaud et al. 2000), mineralisation (van derLinden et al. 2001; Sansalone et al. 2010) and anatomical sites (Ashman et al. 1989; Morgan et al. 2003) on the stiffness of trabecular bone has been discussed in many research works. Bone remodelling (Adachi et al. 2001) also plays a major influence on the apparent stiffness of trabecular bone because the morphology (Karim and Vashishth 2011), mineral contents (Weinans et al. 1992) and biological apatite (BAp) crystallite (Nakano et al. 2005) conditions changed during this process. The changes affected the stiffness of the trabecular bone tissue, and the fluctuations of mineral contents and *c*-axis orientation of BAp caused the trabecular bone tissue to be anisotropic (Tsubota and Adachi 2004). As it was well understood that the apparent mechanical properties are extremely dependent on the bone tissue properties, the estimation of the apparent trabecular bone stiffness should consider these uncertainty factors. Generally speaking, these factors are mainly related to inter-individual differences due to the variations of age (Thomsen et al. 2002) and gender (Wolfram et al. 2010). However, an investigation of the influence of inter-individual differences requires many subjects and specimens. It becomes even more difficult in experimental works because destructive tests are commonly required.

Finite element (FE) methods, and particularly image-based modelling, enable non-destructive evaluation of the apparent mechanical properties of trabecular bone. With the aid of advanced imaging tools now available, realistic trabecular bone models can be generated. However, the reliability and accuracy of the estimation of the mechanical properties is dependent on various factors in image processing. The implication of the image types such as micro-CT, peripheral quantitative computed tomography and magnetic resonance images (van Rietbergen et al. 1998), resolution (Bevill and Keaveny 2009) and threshold value (Hara et al. 2002; Yan et al. 2012) was found to have a major influence on the reconstruction of the trabecular bone model. Hara et al. (2002) reported that even a small variation of the threshold value affected the bone volume fraction and morphological parameters, especially for low bone volume fraction. Moreover, unwanted artefacts (Kopperdahl et al. 2002) and noise (Rajapakse et al.

*Corresponding author. Email: khsalleh@z5.keio.jp; khsalleh@unimap.edu.my

2009) may be generated as part of the trabecular bone model due to uncertainties in image processing, and the affected trabecular connectivity (Kabel et al. 1999) contributes to the fluctuation of apparent mechanical properties.

Nevertheless, in order to consider the random variations of the trabecular bone microstructure caused by various uncertainty parameters, the use of a sampling method or conventional approach of Monte Carlo simulation will require expensive calculation. Therefore, in this study, we present the stochastic multi-scale method applied to trabecular bone volume in order to calculate the variation of the apparent elastic properties of the trabecular bone when considering the uncertainties of *c*-axis BAp orientation due to the bone remodelling process and image-based modelling. The objectives of this study were twofold. First, to investigate the effect of this uncertainty factors on the stochastically apparent elastic moduli of trabecular bone. The second objective was to propose a computational scheme that can improve the prediction of the apparent elastic moduli of trabecular bone when considering uncertainty factors. An extrapolation approach was implemented in the present method by comparing this study with other published experimental results so the reliable results could be predicted.

2. Theoretical framework

Based on the multi-scale theory of a linear problem, the apparent elastic properties of trabecular bone $\mathbf{D^H}$ mainly depend on the geometry of microstructure $\mathbf{X}$ and the microscopic properties of bone tissue $\mathbf{D}$. Variation geometries of the trabecular bone microstructures could possibly be generated with the fluctuations of bone volume fraction V and morphological parameters A. In image-based modelling, the uncertainties of image processing parameters I such as the threshold value and image resolution also affected the geometrical information of the trabecular bone model. Therefore, the estimation of the apparent elastic properties of trabecular bone can be summarised as Equation (1).

$$\mathbf{D^H} = \mathcal{F}(\mathbf{X}(V, A, I), \mathbf{D}), \tag{1}$$

where $\mathcal{F}$ is a function of $\mathbf{D^H}$. In this study, the uncertainties that arise in the geometry of trabecular bone microstructure and microscopic properties of trabecular bone tissue are represented by the variations of image-based modelling and *c*-axis BAp crystallite orientation, respectively.

In this study, the variables which contain random fluctuation at the microscopic scale were denoted by the bold font whereas the plain font expressed the variables for deterministic term. If we assume that the microscopic properties have a small random fluctuation, the stochastic response of $\mathbf{D}$ matrix is characterised by a sum of the deterministic term D^* and a stochastic term that is denoted by α as follows:

$$\mathbf{D} = D^*(1 + \alpha). \tag{2}$$

The stochastic apparent elastic properties can then be formulated as a function of α and approximated in expansion form, as written in the following equation:

$$\mathbf{D^H} = \mathbf{D^H}(\alpha) \approx \sum_k (\mathbf{D^H})^k \phi^k, \tag{3}$$

where ϕ is a fluctuation with kth order. Based on the perturbation theory, ϕ in the equation above is equal to α. The stochastic apparent elastic properties are then rewritten in perturbation form.

$$\mathbf{D^H} = (D^H)^0 + (D^H)^1\alpha + (D^H)^2\alpha^2 + \cdots \tag{4}$$

Considering the fluctuation of α is characterised by the probability density function $f(\alpha)$, an expectation of the apparent elastic properties can be calculated as follows:

$$\begin{aligned} \mathrm{Exp}(\mathbf{D^H}) &= \int_{-\infty}^{\infty} \mathbf{D^H}(\alpha) f(\alpha)\, \mathrm{d}\alpha \\ &\approx \int_{-\infty}^{\infty} \left\{(D^H)^0 + (D^H)^1\alpha + \cdots\right\} f(\alpha)\, \mathrm{d}\alpha. \end{aligned} \tag{5}$$

Applying the first-order perturbation method to this calculation and assuming that the stochastic variable α is in the Gaussian normal distribution range with a mean value of zero, the expected value (Exp) and variance (Var) of the apparent elastic properties are computed in Equations (6) and (7), respectively (Koishi et al. 1996; Sakata et al. 2008).

$$\mathrm{Exp}(\mathbf{D^H}) = (D^H)^0, \tag{6}$$

$$\begin{aligned} \mathrm{Var}(\mathbf{D^H}) &= \int_{-\infty}^{\infty} (\mathbf{D^H}(\alpha) - \mathrm{Exp}(\mathbf{D^H}))^2 f(\alpha)\, \mathrm{d}\alpha \\ &= (D^H)^1 (D^H)^1 \int_{-\infty}^{\infty} \alpha^2 f(\alpha)\, \mathrm{d}\alpha \\ &= (D^H)^1 (D^H)^1 \mathrm{cov}(\alpha, \alpha). \end{aligned} \tag{7}$$

where cov(α,α) is covariance of α. The order of '0' is defined as the deterministic term, whereas '1' corresponds to the first-order differential for the stochastic variation α at $\alpha = 0$.

2.1 A first-order perturbation-based stochastic multi-scale method

Based on the deterministic asymptotic homogenisation theory, the geometrical information $\mathbf{X}$ in Equation (1) is

replaced by the characteristic displacement χ and is written as

$$\mathbf{D^H} = \mathcal{F}(\chi(V, A, I), \mathbf{D}) = \frac{1}{|Y|}\int_Y \mathbf{D}\left(\mathrm{I} - \frac{\partial \chi}{\partial y}\right) \mathrm{d}Y, \quad (8)$$

where $|Y|$ is the volume of the region of interest (ROI) of trabecular bone Y and y denotes the microscopic scale. Then, this equation is discretised using FE methods as

$$\mathbf{D^H} = \frac{1}{|Y|}\int_Y \mathbf{D}\,\mathrm{d}y - \frac{1}{|Y|}\int_Y \mathbf{D}B\chi\,\mathrm{d}y, \quad (9)$$

where B is the strain–displacement matrix. χ is the solution of the microscopic equation and is written in the following linear algebraic form:

$$\mathbf{K}\chi = \mathbf{F} = \int_Y B\hat{\mathbf{D}}\,\mathrm{d}Y, \quad (10)$$

where $\hat{\mathbf{D}}$ is a vector extracted from $\mathbf{D}$ matrix due to heterogeneity at the microscopic scale, based on the asymptotic homogenisation theory (Guedes and Kikuchi 1990). Because the random fluctuation was assumed to arise in $\mathbf{D}$, the stiffness matrix $\mathbf{K}$ and vector $\mathbf{F}$ are approximated using a first-order perturbation as follows:

$$\begin{aligned}\mathbf{K} &\approx K^0 + K^1\alpha \\ &= \int_Y B^{\mathrm{T}}D^0B\,\mathrm{d}Y + \left\{\int_Y B^{\mathrm{T}}\frac{\partial \mathbf{D}}{\partial \alpha}|_{\alpha=0}B\,\mathrm{d}Y\right\}\alpha,\end{aligned} \quad (11)$$

$$\begin{aligned}\mathbf{F} &\approx F^0 + F^1\alpha \\ &= \int_Y \mathbf{B}\hat{D}^0\,\mathrm{d}Y + \left\{\int_Y B\frac{\partial(\hat{D})}{\partial \alpha}|_{\alpha=0}\,\mathrm{d}Y\right\}\alpha.\end{aligned} \quad (12)$$

When the random quantities are inserted into $\mathbf{K}$ and $\mathbf{F}$ in Equation (10), the linear algebraic equation should be rewritten. Therefore, vector χ is also expressed in an approximate form as follows:

$$\chi \approx \chi^0 + \chi^1\alpha. \quad (13)$$

Substituting Equations (11)–(13) into the linear algebraic equation gives the following equation:

$$(K^0 + K^1\alpha)(\chi^0 + \chi^1\alpha) = F^0 + F^1\alpha. \quad (14)$$

By equating the order of α in Equation (14), the solution of the zeroth and first orders of α is calculated as Equations (15) and (16) with a periodic boundary condition.

$$\chi^0 = \left(K^0\right)^{-1}F^0 \quad (15)$$

and

$$\chi^1 = \left(K^0\right)^{-1}(F^1 - K^1\chi^0). \quad (16)$$

Next, using a similar approach we substitute the perturbation form of the $\mathbf{D}$ matrix and the vector χ into Equation (9), which yields

$$\begin{aligned}\mathbf{D^H} = &\frac{1}{|Y|}\int_Y \left(D^0 + D^1\alpha\right)\mathrm{d}y \\ &- \frac{1}{|Y|}\int_Y \left(D^0 + D^1\alpha\right)B\left(\chi^0 + \chi^1\alpha\right)\mathrm{d}y.\end{aligned} \quad (17)$$

Finally, the zeroth and first orders of the stochastically apparent elastic properties can be calculated by equating the order of α, as written in Equations (18) and (19), respectively, as follows:

$$(D^H)^0 = \frac{1}{|Y|}\int_Y D^0\,\mathrm{d}y - \frac{1}{|Y|}\int_Y D^0B\chi^0\,\mathrm{d}y, \quad (18)$$

$$\begin{aligned}(D^H)^1 = &\frac{1}{|Y|}\int_Y D^1\,\mathrm{d}y \\ &- \frac{1}{|Y|}\int_Y \left(D^0B\chi^1 + D^1B\chi^0\right)\mathrm{d}y.\end{aligned} \quad (19)$$

Each order of $\mathbf{D^H}$ is applied to Equations (7) and (8) in order to obtain the expected value and variance of the apparent elastic properties. The apparent elastic properties derived here are in tensor matrix form. In order to obtain the stochastic apparent elastic moduli, the inverse of the tensor matrix form was then derived. The details of the derivation are available in Appendix A.

2.2 *Uncertainty of BAp crystallite orientation*

Due to the bone remodelling process, uncertainty arises in trabecular stiffness orientation that results from the preferential alignment of the c-axis of the BAp crystallite. The trabecular stiffness in the c-axis is almost twice as high than the stiffness in the other two orthogonal axes (Miyabe et al. 2007). Therefore, we use the stochastic anisotropy in the material axes of the trabecular bone. Probability density of the c-axis orientation with respect to the trabecular bone tissue axis is assumed in normal distribution and the mean axis is aligned at axis-2 (which is the principal axis of trabecular bone network), as shown in Figure 1(a). Due to the fluctuation of c-axis orientation, Young's modulus of trabecular bone tissue in axis-2, $\mathbf{E}_2$, is also scattered in normal distribution with the mean value at E^0 as illustrated in Figure 1(b). Hence, the stochastic response of $\mathbf{E}_2$ is written as follows:

$$\mathbf{E}_2 = E^0(1 + \alpha), \quad (20)$$

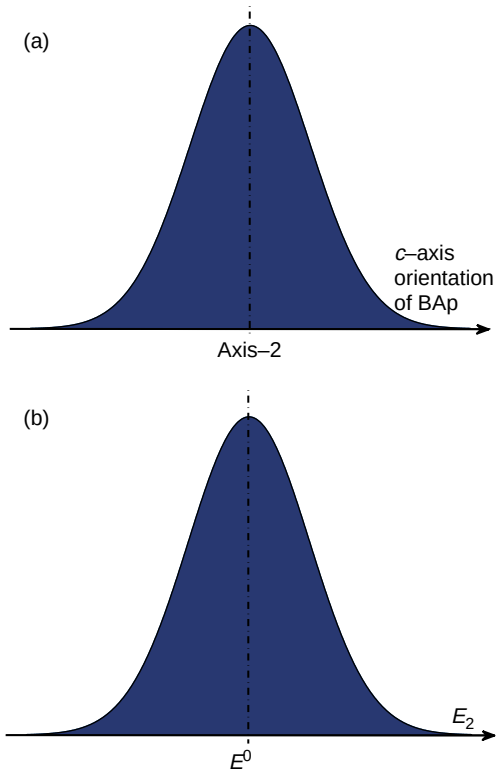

Figure 1. Probability of Young's modulus of trabecular bone tissue in the principal axis with respect to the fluctuation of *c*-axis orientation of BAp. (a) Probability density of *c*-axis orientation of BAp along the trabecular bone tissue axis. (b) Probability density of Young's modulus in the principal axis (axis-2).

where E^0 denotes the deterministic Young's modulus of bone tissue. We then set Young's modulus in the two other orthogonal directions ($\mathbf{E}_1$ and $\mathbf{E}_3$) as Equation (21) to hold the transverse-isotropic characteristic in the microscopic properties of trabecular bone.

$$\mathbf{E}_1 = \mathbf{E}_3 = \frac{\mathbf{E}_2}{2} = \frac{E^0(1+\alpha)}{2}. \tag{21}$$

In order to maintain the symmetry of the compliance matrix $\mathbf{C}_{ij}$, we express the deterministic Poisson's ratio ν and shear modulus $\mathbf{G}$ as Equations (22) and (23), respectively.

$$\nu_{13} = \nu_{12} = \nu_{31} = \nu_{32} = \nu \quad \text{and} \quad \nu_{21} = \nu_{23} = \frac{\nu}{2}, \tag{22}$$

$$\mathbf{G}_{23} = \mathbf{G}_{31} = \mathbf{G}_{12} = \frac{E^0(1+\alpha)}{2(1+\alpha)}. \tag{23}$$

Next, the microscopic elastic tensor $\mathbf{D}_{ij}$ is obtained by taking the inverse of the compliance matrix. The stochastic variable that considers the fluctuation of Young's modulus due to *c*-axis orientation in trabecular bone is imposed in the $\mathbf{D}$ matrix. The derivation of the stochastic $\mathbf{C}_{ij}$ and $\mathbf{D}_{ij}$ matrices is available in Appendix B.

2.3 *Uncertainty of image-based modelling*

Considering uncertainties in image processing, variations of image-based models could be constructed. However, in order to propose effective apparent elastic properties of trabecular bone considering the variation of image-based constructed models, we assume that the probability of the models is determined by a probability function $f(I)$ that is characterised in normal distribution and shown in Figure 2. The probability of the models PrI is calculated by taking the integration of $f(I)$, then each probability of I (divided with the same interval) is obtained using the empirical rule of normal distribution, as shown in Figure 2 and written in Equation (24).

$$\Pr I = \int_I f(I)\,\mathrm{d}I \approx \sum_{i=1}^{N} (\Pr I)_i = 1, \tag{24}$$

where i is the ith number of image-based models and N is the total number of image-based models that are considered.

The Gaussian mixture model is then used to obtain a unique solution considering the variation of image-based models. If the probability of I is assumed as a weighted w sum of N component Gaussian densities $g_{(\mu,\sigma^2)}$ (with mean value μ and variance σ^2), the effective stochastically apparent elastic properties of trabecular bone $\mathbf{D}^{\mathbf{H}(\text{eff.})}$ are calculated as Equation (25).

$$\mathbf{D}^{\mathbf{H}(\text{eff.})} = \sum_{i=1}^{N} w_i \left(g_{(\mu,\sigma^2)}\right)_i = \sum_{i=1}^{N} (\Pr I)_i (\mathbf{D}^{\mathbf{H}})_i. \tag{25}$$

2.4 *Influence of inter-individual difference*

Generally speaking, the variation of trabecular bone characteristics is correlated with the inter-individual difference factor. In order to estimate the reliable apparent mechanical properties, for instance when considering multiple age and gender for certain bone density, a huge amount of tests are required. Even with these tests, it is difficult to obtain the same bone density from different

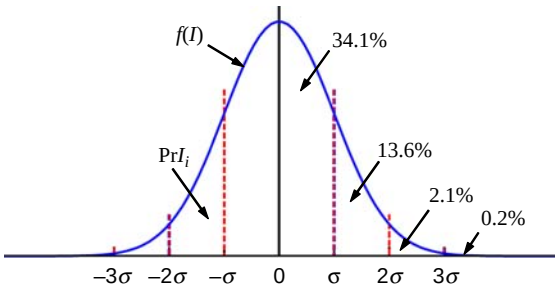

Figure 2. Probability (PrI) of image-based models.

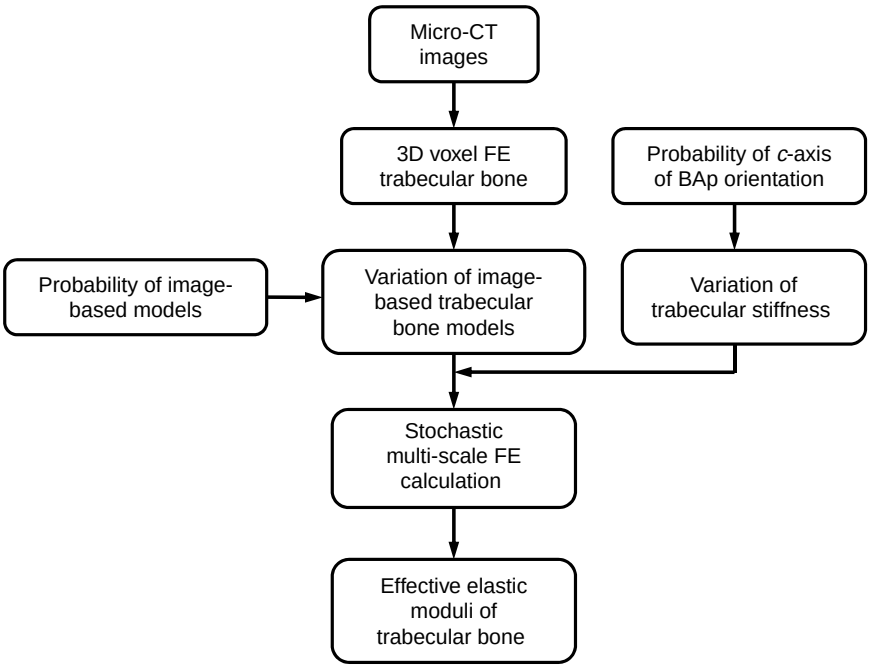

Figure 3. The implementation of this study.

individuals. Therefore, we introduce the coefficient factor β in the present approximation in order to characterise the dispersion of the prediction due to inter-individual difference, as written as follows:

$$\mathbf{D^H} = (D^H)^0 + \beta(D^H)^1\alpha, \tag{26}$$

where β is a scalar value that represents the scale of the fluctuation in the apparent elastic properties of trabecular bone. The appropriate value of β is predicted using the extrapolation approach by comparing it with the published experimental results from other studies.

3. Modelling and computational implementation

The implementation of the present theoretical framework is shown in Figure 3. The micro-FE model of trabecular bone was reconstructed using a micro-CT image. The fourth lumbar (L4) vertebral trabecular bone was extracted from a male cadaver aged 69 years old which was donated by Osaka City University Hospital. Based on dual-energy X-ray absorptiometry analysis, the cadaver had not suffered from metabolic bone disease. The Ethics Committee approved the analysis of this bone. The bone specimen was examined using a micro-CT device (SMX-100CT; Shimadzu, Kyoto, Japan) with a voltage of 40 kV

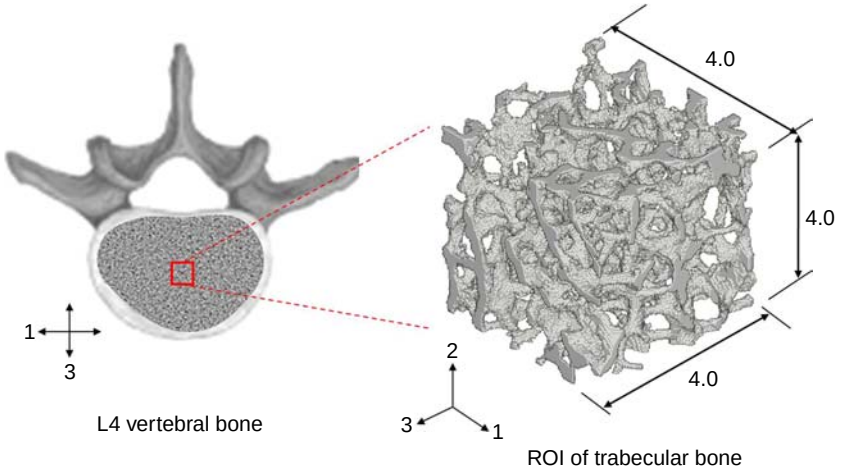

Figure 4. Location and dimension (in mm) of extracted ROI from L4 vertebral trabecular bone specimen.

Table 1. Characteristics of the image-based modelling treatments.

I	Image-based modelling process	No. of voxel elements	BV/TV[a]
1	Labelling	455,531	0.1524
2	Labelling → voxel edge → labelling	459,951	0.1530
3	Labelling → dilation → erosion → labelling	465,426	0.1567
4	Labelling → dilation → erosion → voxel edge → labelling	465,811	0.1569
5	Labelling → dilation × 2 → erosion × 2 → labelling	481,568	0.1637
6	Labelling → dilation × 2 → erosion × 2 → voxel edge → labelling	481,885	0.1639
7	Labelling → dilation × 3 → erosion × 3 → labelling	505,965	0.1744
8	Labelling → dilation × 3 → erosion × 3 → voxel edge → labelling	506,213	0.1746

[a] Bone volume fraction.

and a current of 30 μA. The resolution of the micro-CT image was 30 μm and the slice thickness of the micro-CT was chosen the same as in the in-plane resolution.

The three-dimensional (3D) trabecular bone model was reconstructed using a binarised micro-CT image. The threshold of the segmentation image was determined by comparing the specific portion of the binarised trabecular microstructure image with the cross section of real bone slice. The voxel FE model was generated by converting slices of trabecular bone images (Hollister and Kikuchi 1994). The element size was set equal to micro-CT image resolution such that voxels in the resulting reconstructions were equally sized in all spatial directions. The ROI was selected at the central part of the L4 vertebral body, as shown in Figure 4. The selection of ROI is important because the size and geometry of the ROI have an effect on the final result (Huet 1990; Linde et al. 1992). The ROI was carefully selected in order to hold the periodicity by ensuring the areal bone density consistent along all three cross-sectional areas and at the boundaries. The volume fraction or bone volume over total volume (BV/TV) of ROI was calculated to be 15.24% in a cube of 4.0 mm × 4.0 mm × 4.0 mm by the author's original software, named DoctorBQ (Tokyo, Japan). The size satisfied the requirements of at least five intertrabecular lengths (Harrigan et al. 1987). Left-right, vertical and anteroposterior axes were defined as axes 1, 2 and 3, respectively. Young's modulus of bone tissue E^0 was set as 10 GPa (Rho et al. 1993) and 0.4 of Poisson's ratio. A periodic boundary condition was applied to the ROI in order to eliminate possible errors due to the boundary condition setting (Ladd and Kinney 1998). The fluctuation of the *c*-axis orientation that was denoted by α was assumed to be in normal distribution with a zero mean value and variance of 0.03. The value of variance was recommended to be below 0.1 in order to keep the accuracy using the approximation of perturbation method (Kaminski and Kleiber 2000).

In this study, we introduced eight image-based modelling treatments *I* to construct a variation of trabecular bone models that could possibly be generated due to the uncertainty of the image processing techniques. These treatments were proposed to compensate for the broken or interconnected trabecular bone images that might happen because of inappropriate image resolution, the existence of noise and artefacts or any errors during the imaging process. The characteristics of the image-based modelling treatments are listed in Table 1. The labelling process was implemented in order to eliminate the noises and artefacts that exist after the reconstruction of the 3D model. In the voxel edge process, for each two voxel elements that were only connected at one edge, the other two neighbouring voxel elements were generated. The −2D illustration of this process is shown in Figure 5(a). Figure 5(b)–(d) illustrates the possible outcome models that could be created when performing the dilation–erosion process. Figure 6 shows the reconstructed

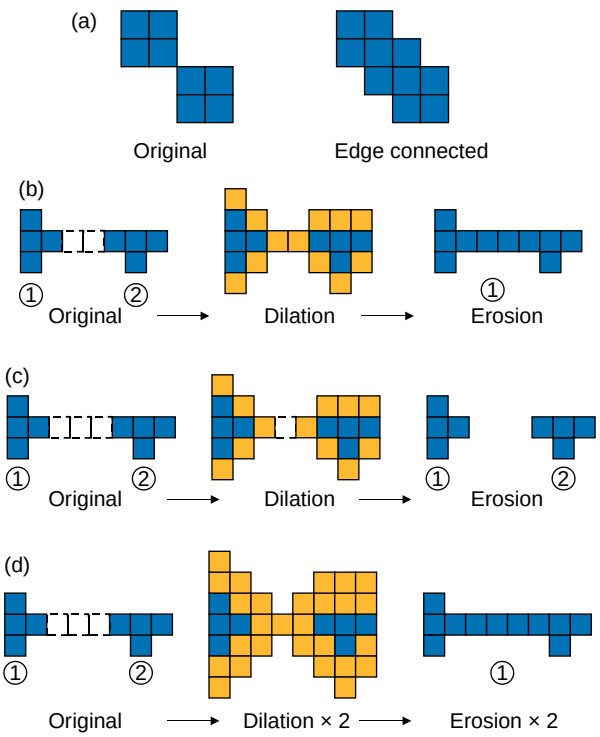

Figure 5. Illustration of 2D voxel elements subjected to image-based modelling treatments. (a) voxel edge, (b) dilation → erosion (connected), (c) dilation → erosion (not connected) and (d) dilation × 2 → erosion × 2 (connected).

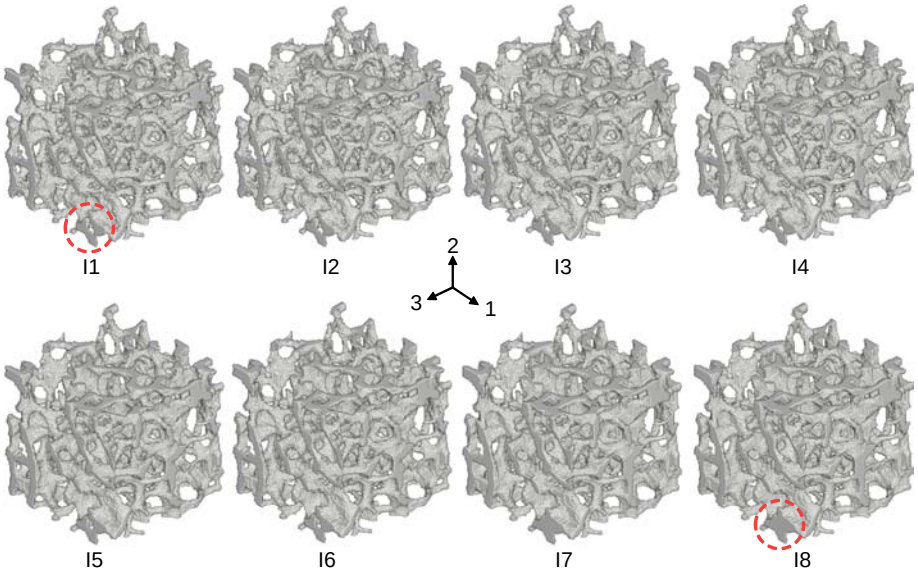

Figure 6. Reconstructed trabecular bone models under eight image-based modelling treatments.

trabecular bone models according to the treatments proposed in Table 1. At a glance, it was difficult to identify the differences of each case, but by comparing the circle marked part in ROIs *I*1 and *I*8, the changes were seen.

The effective apparent elastic moduli of trabecular bone when considering the uncertainties of the *c*-axis of BAp crystallite orientation and image-based modelling was then computed using the stochastic multi-scale method as described in Section 2. Finally, we compared the result with other published experimental works as listed in Table 2 in order to predict the coefficient factor that could characterise the inter-individual difference factor. The comparison was made with respect to the equivalent bone density as proposed by Keyak et al. (1994). The experiment result obtained by Keyak et al. (1994) has been widely used for comparison with FE analysis. Therefore, the calculated apparent Young's modulus in the principal axis was plotted on Keyak et al.'s (1994) result, and the feature of the Keyak et al.'s experimental result was examined.

4. Results

The effect of the image-based modelling process on the dispersion of apparent Young's modulus $\mathbf{E}^{\mathbf{H}}$ in axes 1, 2 and 3 due to the fluctuation of the *c*-axis of BAp crystallite orientation is shown in Figure 7. The error bar indicates the standard deviation of apparent Young's modulus. The stiffness was increased with respect to the increment of minor changes in the image-based modelling process. The increment rate of $\mathbf{E}^{\mathbf{H}}$ appeared larger for the dilation–erosion process than for the voxel-edge process. The $\mathbf{E}^{\mathbf{H}}$ at *I*8 was increased by almost 50% compared with that at *I*1 in all axes. It was noted that the expected value of $\mathbf{E}^{\mathbf{H}}_{22}$ was almost four times larger than $\mathbf{E}^{\mathbf{H}}_{11}$ and three times larger than $\mathbf{E}^{\mathbf{H}}_{33}$ for all *I*'s. The results suggest that the apparent elastic moduli of trabecular bone were sensitive to the image-based modelling, although only minor adjustments were made to the model. In the same manner, Figure 8 shows the effect of *I* on the variation of the apparent shear modulus for $\mathbf{G}^{\mathbf{H}}_{23}$, $\mathbf{G}^{\mathbf{H}}_{31}$ and $\mathbf{G}^{\mathbf{H}}_{12}$. A pattern similar to the apparent Young's modulus was found in the apparent shear

Table 2. Other published experimental results on the estimation of apparent Young's modulus of trabecular bone in the vertical axis.

No.	Authors (year)	Anatomic site	$E = f(\rho)$[a]	r[b]	Density type
1	Hvid et al. (1989)	Tibia	$2132\rho^{1.46}$	0.78	Dry
2	Linde and Hvid (1989)	Tibia	$10256\rho^{2.5}$	0.92	Dry
3	Odgaard and Linde (1991)	Tibia	$23500\rho^{2.1}$	0.85	Ash
4	Linde et al. (1992)	Tibia	$4778\rho^{1.99}$	0.89	Dry
5	Keyak et al. (1994)	Tibia	$33900\rho^{2.2}$	0.92	Ash
6	Kopperdahl and Keaveny (1998)	Vertebra	$2350\rho^{1.2}$	0.93	Dry
7	Morgan et al. (2003)	Vertebra	$4730\rho^{1.56}$	0.93	Dry

[a] Young's modulus E in MPa and apparent density ρ in g/cm^3.
[b] Correlation coefficient of regression equation.

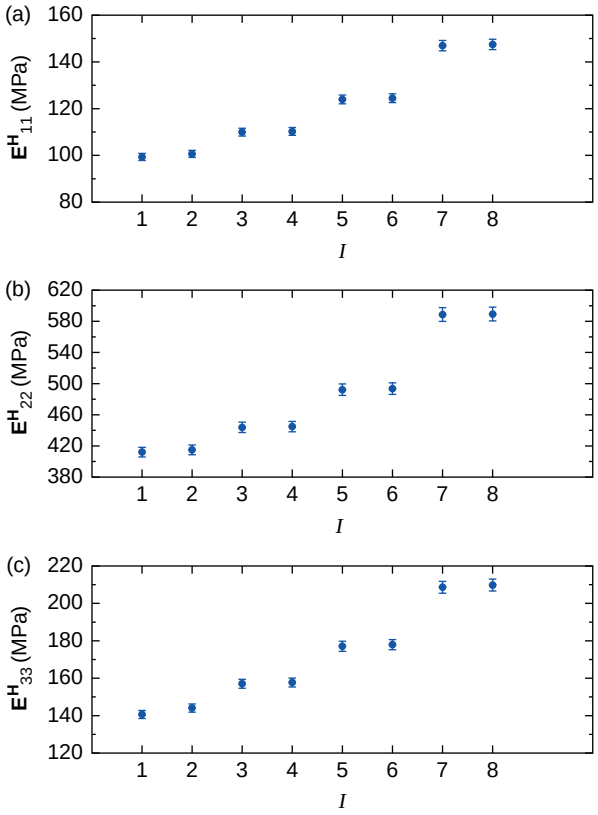

Figure 7. The effect of image-based modelling treatments on the stochastically apparent Young's moduli.

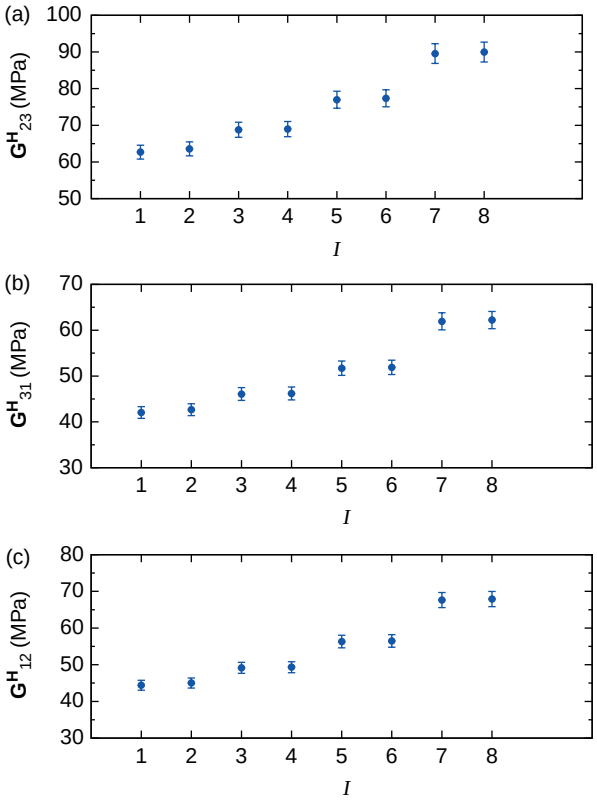

Figure 8. The effect of image-based modelling treatments on the stochastically apparent shear moduli.

moduli. The $\mathbf{G}^{\mathbf{H}}_{23}$ was the highest apparent shear modulus of the present ROI. Contrary to this, the apparent Poisson's ratio $\nu^{\mathbf{H}}$ was not sensitive to the changes of I, as shown in Figure 9. Although $\nu^{\mathbf{H}}_{32}$ shows some increments with respect to the changes of I, the value was relatively very small.

Considering that the probability of I is in normal distribution and the summation of the distributions is determined by the Gaussians mixture model, the effective apparent elastic modulus of trabecular bone is then obtained. The mean value of other published experimental works (based on their regression equations) against the equivalent bone density for the apparent Young's modulus in the vertical axis ($\mathbf{E}^{\mathbf{H}}_{22}$) is plotted at $\beta = 8$, as shown in Figure 10. The predicted result was found to be in good agreement with other experimental results. The appropriate value of β was estimated based on the extrapolation of other experimental results. Our result in distribution form covered the scattering of other results with the mean value, which was obtained at approximately 460 MPa. Although our mean value was found to be underestimated when compared to the mean value of Keyak et al.'s (1994) experimental result, however the original experimental plots show surprising dispersal in large bounds, as displayed in Figure 11. Our estimated apparent Young's modulus covered only the average and lower bound of Keyak et al.'s (1994) experimental result, but this was far from the upper bound. It suggests that the experimental works produced the large scattered result, and the approximated regression equation could not give meaningful predictions with respect to certain bone density.

5. Discussion

The apparent elastic moduli of trabecular bone are predicted in stochastic nature when considering the uncertainties of trabecular bone stiffness orientation and image-based modelling. It appeared that the apparent elastic properties of trabecular bone are sensitive to image processing although only minor adjustment was done on the trabecular bone model. Similar findings may have been reported in the past, such as the effect of image threshold (Hara et al. 2002; Yan et al. 2012), noise and resolution (Rajapakse et al. 2009) on the trabecular stiffness, but the image-based modelling steps that are introduced here are intended to compensate for the connectivity of the trabecular network that may break or disappear due to uncertainty in the image processing procedure, especially for the case of thin trabecular struts. Our result suggests

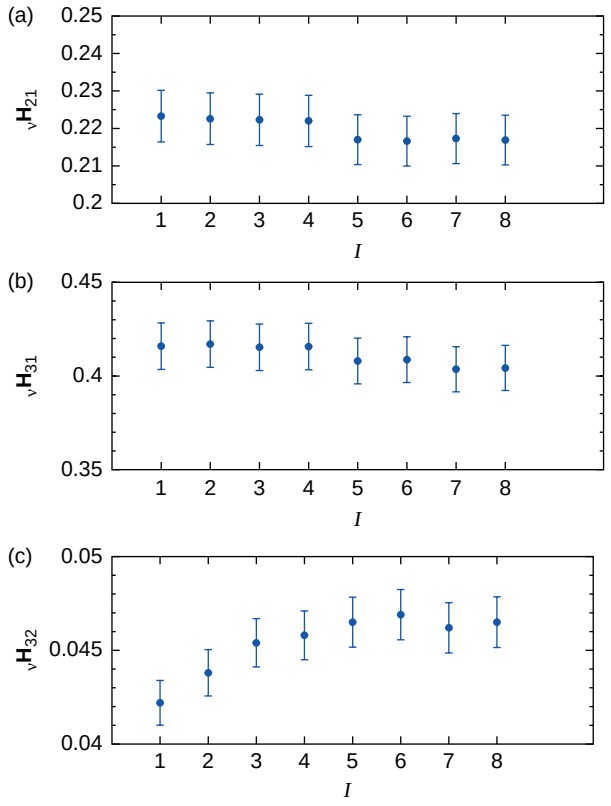

Figure 9. The effect of image-based modelling treatments on the stochastically apparent Poisson's ratio.

that even a minor improvement on the connectivity increased the apparent stiffness of trabecular bone, and this is consistent with other literature (Kinney and Ladd 1998; Kabel et al. 1999). However, the effect of fluctuation of trabecular stiffness orientation on the apparent elastic moduli is hardly seen by observing the standard deviation in the present result (Figures 7 and 8). This is because of the limitation of a first-order perturbation method, in which the random fluctuation of α should be small and the standard deviation of the fluctuation was recommended to be lower than 0.1 (Kaminski 2009). However, approximation using a first-order perturbation can provide an accurate result for Young's modulus variation, but estimations considering Poisson's ratio variation should require higher order expansions (Sakata et al. 2008). Sakata et al. (2008) reported that higher order approximation does not always improve the accuracy of the stochastic estimations, especially for Young's moduli that exhibit variations (Sakata et al. 2008). Therefore, only Young's modulus was assumed to have a fluctuation due to the uncertainty of *c*-axis BAp orientation in this study.

According to the results (Figures 7 and 8), the small fluctuation on the uncertainty parameters at micro-scale level produced dispersion of the apparent elastic moduli. The variation of the estimated result might be increased if other uncertainty factors due to bone characteristics or inter-individual differences are considered. In the present method, the effective apparent elastic modulus of trabecular bone was predicted by considering inter-individual differences using the extrapolation approach to other experimental results. Rather than undertaking

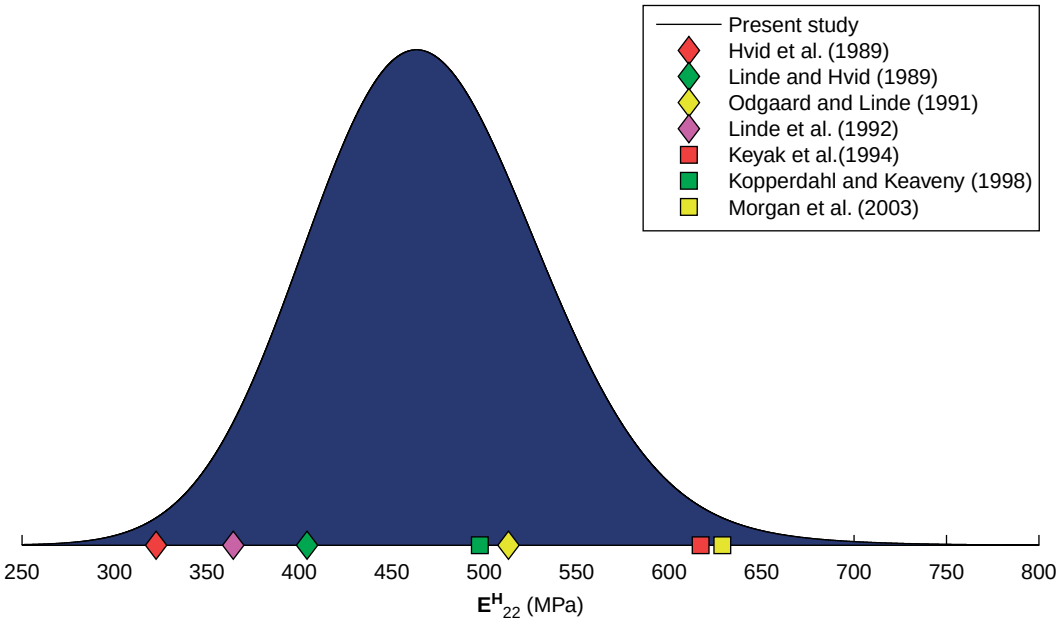

Figure 10. The effective apparent Young's modulus in the vertical axis with other past results.

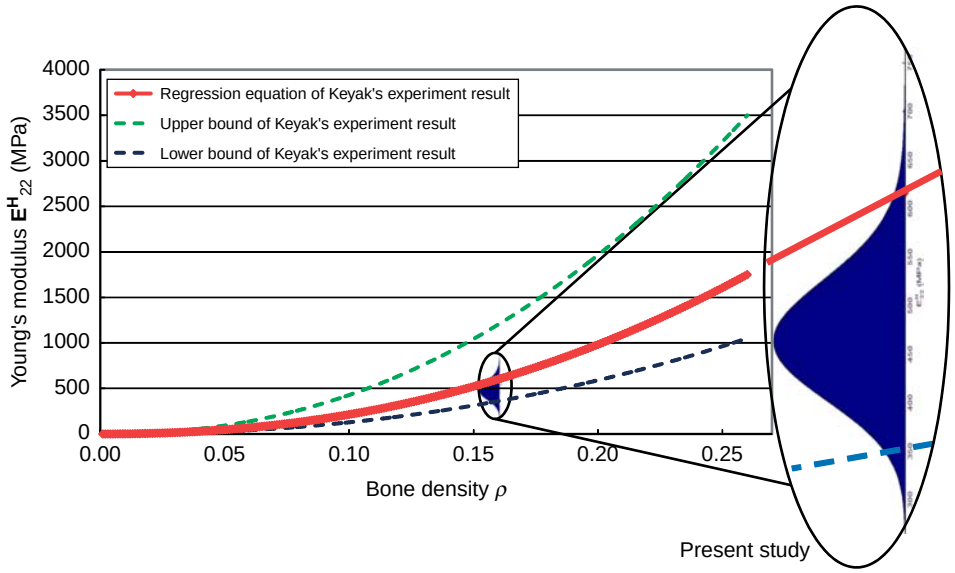

Figure 11. The estimated effective apparent Young's modulus in the vertical axis on Keyak et al.'s experimental result.

many tests from various individuals, the introduction of β could characterise the inter-individual differences and improve the reliability of the prediction.

Moreover, the mean value provided by the regression equation of other experimental results could not describe the real behaviour of the measured value. Difficulty may lie in predicting the reliable apparent elastic modulus with respect to certain bone density from a huge dispersed result obtained by the experiment, as illustrated in Figure 11. The reliability of the experimental result is not a matter of concern in this case, but the improved evaluation procedure should be considered rather than the regression equation in order to give a meaningful prediction of the trabecular stiffness with respect to bone volume fraction. For instance, our estimation in the distribution form is able to give a guideline to evaluate the measured data. The distribution curve could be represented as a weight or percentage of reliability of the measured value. The measured value nearest to the mean value should have more weightage than the value near to the upper and lower bounds.

The present method provides additional insight in order to predict more reliable apparent elastic moduli of trabecular bone, because as many uncertainty parameters as possible were taken into account. Other possible errors that are commonly highlighted in the previous studies such as discretisation (Ulrich et al. 1998), boundary conditions (Ladd and Kinney 1998) and ROI size (Choi et al. 1990) are minimised in this study. Chevalier et al. (2007) reported the voxel-based FE with the size of 30–45 μm^3 is appropriate for linear elastic analysis, and the validation of this FE size was carried out by comparison with the results of mechanical tests and nanoindentation. Although the discontinuity easily happens at the boundary of trabecular struts due to the shape of the voxel elements, the use of a voxel edge process in the present method improved the smoothness of the trabecular geometry. The error caused by boundary conditions in numerical modelling is eliminated when the periodic boundary condition [as proposed to the asymptotic homogenisation theory (Hollister et al. 1991)] was applied. The ROI was also carefully selected to hold the periodicity using the specific computational tool (DoctorBQ), and the size satisfied the requirements for the appropriate numerical test (Harrigan et al. 1987).

Some limitations associated with this study should be noted when evaluating the present results. First, only a single ROI was extracted from an L4 vertebral trabecular bone specimen. As this is the first attempt of using the proposed method, more emphasis was put on the applicability of the algorithm applied to the apparent stiffness of trabecular bone estimation. It may be necessary in the future to apply the present method to various features or microarchitectures of ROIs with different bone volume fractions in order to draw more general conclusions. The additional data using this method may help to propose the unique solution of the coefficient factor as presented in this study. We expect the coefficient factor that corresponds to the inter-individual difference should be a function of bone volume fraction in the future. Second, this study is limited to linear elastic analysis because the trabecular bone image was captured from the dried bone. The existence of mineralisation is neglected. Although the tissue mineralisation is inhomogeneous, the results of previous studies (Jaasma et al. 2002; Gross et al. 2012) suggest that the effects of inhomogeneous mineralisation on the strength of the trabecular bone are likely very small. Third, the fluctuation of microscopic

properties and image-based models is assumed to be in normal distribution. The normal distribution was chosen to characterise the fluctuation in our stochastic computational scheme because no probabilistic experimental results are currently available on bone tissue modulus. It will be in our future interest to test the method on various types of probabilistic density functions.

In the future, we expect the method developed here could potentially provide relevant and detailed information about the reference in predicting and evaluating realistic elastic moduli of trabecular bone.

6. Conclusions

The stochastic computational method used to estimate the variation of apparent elastic moduli of trabecular bone when considering the uncertainties primarily due to trabecular stiffness orientation and image-based modelling was presented in this study. The apparent elastic modulus was found to be sensitive to the connectivity of the trabecular bone network that is influenced by the image processing. The reliability of the prediction was improved by introducing the coefficient factor of β to represent various bone characteristics due to inter-individual differences.

Acknowledgements

The authors would like to thank Prof. Yuji Nakajima and Prof. Hiroshi Kiyama (Osaka City University) for providing the bone specimen. We also wish to thank the donor's family for their generosity in the face of their bereavement. Next, the dedicated help from Dr Takuya Ishimoto and Dr Sayaka Miyabe (both from Osaka University) in preparing the micro-CT images for this research is acknowledged with gratitude. This study was also supported in part by the Ministry of Higher Education (MOHE), Malaysia under a Scholarship for Academicians Training Scheme.

References

Adachi T, Tsubota Ki, Tomita Y, Hollister SJ. 2001. ASME; Trabecular surface remodeling simulation for cancellous bone using microstructural voxel finite element models. J Biomech Eng. 123(5):403–409.

Ashman RB, Rho JY, Turner CH. 1989. Anatomical variation of orthotropic elastic moduli of the proximal human tibia. J Biomech. 22(8–9):895–900.

Bevill G, Keaveny TM. 2009. Trabecular bone strength predictions using finite element analysis of micro-scale images at limited spatial resolution. Bone. 44(4):579–584.

Carter DR, Hayes WC. 1977. The compressive behavior of bone as a two-phase porous structure. J Bone Joint Surg. 59(7):954–962.

Chevalier Y, Pahr D, Allmer H, Charlebois M, Zysset P. 2007. Validation of a voxel-based FE method for prediction of the uniaxial apparent modulus of human trabecular bone using macroscopic mechanical tests and nanoindentation. J Biomech. 40(15):3333–3340.

Choi K, Kuhn JL, Ciarelli MJ, Goldstein SA. 1990. The elastic moduli of human subchondral, trabecular, and cortical bone tissue and the size-dependency of cortical bone modulus. J Biomech. 23:1103–1113.

Dempster DW. 2000. The contribution of trabecular architecture to cancellous bone quality. J Bone Mineral Res. 15(1):20–23.

Gross T, Pahr DH, Peyrin F, Zysset PK. 2012. Mineral heterogeneity has a minor influence on the apparent elastic properties of human cancellous bone: a SRμCT-based finite element study. Comput Meth Biomech Biomed Eng. 15(11):1137–1144.

Guedes J, Kikuchi N. 1990. Preprocessing and postprocessing for materials based on the homogenization method with adaptive finite element methods. Comput Meth Appl Mech Eng. 83(2):143–198.

Hara T, Tanck E, Homminga J, Huiskes R. 2002. The influence of microcomputed tomography threshold variations on the assessment of structural and mechanical trabecular bone properties. Bone. 31(1):107–109.

Harrigan TP, Jasty M, Mann RW, Harris WH. 1987. Limitation of the continuum assumption in cancellous bone. J Biomech. 21(4):269–275.

Hollister SJ, Fyhrie DP, Jepsen KJ, Goldstein SA. 1991. Application of homogenization theory to the study of trabecular bone mechanics. J Biomech. 24(9):825–839.

Hollister SJ, Kikuchi N. 1994. A Wiley Company; Homogenization theory and digital imaging: a basis for studying the mechanics and design principles of bone tissue. Biotechnol Bioeng. 43(7):586–596.

Huet C. 1990. Application of variational concepts to size effects in elastic heterogeneous bodies. J Mech Phys Solids. 38(6):813–841.

Hvid I, Bentzen SrM, Linde F, Mosekilde L, Pongsoipetch B. 1989. X-ray quantitative computed tomography: the relations to physical properties of proximal tibial trabecular bone specimens. J Biomech. 22(8–9):837–844.

Jaasma MJ, Bayraktar HH, Niebur GL, Keaveny TM. 2002. Biomechanical effects of intraspecimen variations in tissue modulus for trabecular bone. J Biomech. 35(2):237–246.

Kabel J, Odgaard A, van Rietbergen B, Huiskes R. 1999. Connectivity and the elastic properties of cancellous bone. Bone. 24(2):115–120.

Kaminski M. 2009. Sensitivity and randomness in homogenization of periodic fiber-reinforced composites via the response function method. Int J Solids Struct. 46(3–4):923–937.

Kaminski M, Kleiber M. 2000. Perturbation based stochastic finite element method for homogenization of two-phase elastic composites. Comput Struct. 78(6):811–826.

Karim L, Vashishth D. 2011. Role of trabecular microarchitecture in the formation, accumulation, and morphology of microdamage in human cancellous bone. J Orthop Res. 29(11):1–6.

Keyak JH, Lee IY, Skinner HB. 1994. Correlations between orthogonal mechanical properties and density of trabecular bone: use of different densitometric measures. J Biomed Mater Res. 28(11):1329–1336.

Kinney JH, Ladd AJC. 1998. The relationship between three-dimensional connectivity and the elastic properties of trabecular bone. J Bone Mineral Res. 13(5):839–845.

Koishi M, Shiratori M, Miyoshi T, Miyano A. 1996. Stochastic homogenization method for composite materials with uncertain microstructures. Trans Jpn Soc Mech Eng A. 62:2264–2269.

Kopperdahl DL, Keaveny TM. 1998. Yield strain behavior of trabecular bone. J Biomech. 31(7):601–608.
Kopperdahl DL, Morgan EF, Keaveny TM. 2002. Quantitative computed tomography estimates of the mechanical properties of human vertebral trabecular bone. J Orthop Res. 20(4):801–805.
Ladd AJ, Kinney JH. 1998. Numerical errors and uncertainties in finite-element modeling of trabecular bone. J Biomech. 31(10):941–945.
Linde F, Hvid I. 1989. The effect of constraint on the mechanical behaviour of trabecular bone specimen. J Biomech. 22(5):485–490.
Linde F, Hvid I, Madsen F. 1992. The effect of specimen geometry on the mechanical behaviour of trabecular bone specimens. J Biomech. 25(4):359–368.
Miyabe S, Nakano T, Ishimoto T, Takano N, Adachi T, Iwaki H, Kobayashi A, Takaoka K, Umakoshi Y. 2007. Two-dimensional quantitative analysis of preferential alignment of bap *c*-axis for isolated human trabecular bone using microbeam X-ray diffractometer with a transmission optical system. Mater Trans. 48(3):343–347.
Morgan EF, Bayraktar HH, Keaveny TM. 2003. Trabecular bone modulus-density relationships depend on anatomic site. J Biomech. 36(7):897–904.
Nakano T, Ishimoto T, Umakoshi Y, Tabata Y. 2005. Texture of biological apatite crystallites and the related mechanical function in regenerated and pathological hard tissues. J Hard Tissue Biol. 14(4):363–364.
Odgaard A, Linde F. 1991. The underestimation of Young's modulus in compressive testing of cancellous bone specimens. J Biomech. 24(8):691–698.
Pothuaud L, Porion P, Lespessailles E, Benhamou CL, Levitz P. 2000. A new method for three-dimensional skeleton graph analysis of porous media: application to trabecular bone microarchitecture. J Microsc. 199(Part 2):149–161.
Rajapakse CS, Magland J, Zhang XH, Liu XS, Wehrli SL, Guo XE, Wehrli FW. 2009. Implications of noise and resolution on mechanical properties of trabecular bone estimated by image-based finite-element analysis. J Orthop Res: Official Publication of the Orthop Res Soc. 27(10):1263–1271.
Rho JY, Ashman RB, Turner CH. 1993. Young's modulus of trabecular and cortical bone material: ultrasonic and microtensile measurements. J Biomech. 26(2):111–119.
Sakata S, Ashida F, Kojima T, Zako M. 2008. Three-dimensional stochastic analysis using a perturbation-based homogenization method for elastic properties of composite material considering microscopic uncertainty. Int J Solids Struct. 45(3–4):894–907.
Sansalone V, Naili S, Bousson V, Bergot C, Peyrin F, Zarka J, Laredo JD, Haïat G. 2010. Determination of the heterogeneous anisotropic elastic properties of human femoral bone: from nanoscopic to organ scale. J Biomech. 43(10):1857–1863.
Thomsen JS, Ebbesen EN, Mosekilde Li. 2002. Age-related differences between thinning of horizontal and vertical trabeculae in human lumbar bone as assessed by a new computerized method. Bone. 31(1):136–142.
Tsubota Ki, Adachi T. 2004. Changes in the fabric and compliance tensors of cancellous bone due to trabecular surface remodeling, predicted by a digital image-based model. Comput Meth Biomech Biomed Eng. 7(4):187–192.
Ulrich D, van Rietbergen B, Weinans H, Rüegsegger P. 1998. Finite element analysis of trabecular bone structure: a comparison of image-based meshing techniques. J Biomech. 31(12):1187–1192.
van derLinden JC, Birkenhäger-Frenkel DH, Verhaar JAN, Weinans H. 2001. Trabecular bone's mechanical properties are affected by its non-uniform mineral distribution. J Biomech. 34(12):1573–1580.
van Rietbergen B, Majumdar S, Pistoia W, Newitt DC, Kothari M, Laib A, Rugsegger P. 1998. Assessment of cancellous bone mechanical properties from micro-FE models based on micro-CT, pQCT and MR images. Technol Health Care. 6(5–6):413–420.
Weinans H, Huiskes R, Grootenboer HJ. 1992. The behavior of adaptive bone-remodeling simulation models. J Biomech. 25(12):1425–1441.
Wolfram U, Wilke HJ, Zysset PK. 2010. Transverse isotropic elastic properties of vertebral trabecular bone matrix measured using microindentation under dry conditions (effects of age, gender, and vertebral level). J Mech Med Biol. 10(01):139–150.
Yan YB, Qi W, Tianxia Q, Teo EC, Lei W. 2012. The effect of threshold value on the architectural parameters and stiffness of human cancellous bone in micro ct analysis. J Mech Med Biol. 12(5):1–16.

Appendix A: Derivation of the stochastic apparent elastic moduli

A.1 Compliance matrix of the stochastically apparent elastic properties

The first-order approximation of the stochastically apparent elastic properties can be written as

$$\mathbf{D}^{\mathbf{H}}_{ij} = \left(D^{H0}_{ij}\right) + \left(D^{H1}_{ij}\right)\alpha. \tag{A1}$$

Taking the inverse, we obtain (for $i,j = 1–3$)

$$\left(\mathbf{D}^{\mathbf{H}}_{ij}\right)^{-1} = \mathbf{C}^{\mathbf{H}}_{ij} = \frac{1}{|\mathbf{D}^{\mathbf{H}}|}\begin{bmatrix} c_{11} & c_{12} & c_{13} \\ c_{21} & c_{22} & c_{23} \\ c_{31} & c_{32} & c_{33} \end{bmatrix}, \tag{A2}$$

where

$$|\mathbf{D}^{\mathbf{H}}| = \left(D^{H0}_{11} + D^{H1}_{11}\alpha\right)\left(D^{H0}_{22} + D^{H1}_{22}\alpha\right)\left(D^{H0}_{33} + D^{H1}_{33}\alpha\right) + \cdots \tag{A3}$$

The approximation up to the first order of α yields

$$|\mathbf{D}^{\mathbf{H}}| = \left(D^{H0}_{11}D^{H0}_{22}D^{H0}_{33} + \cdots\right) + \left(D^{H1}_{11}D^{H0}_{22}D^{H0}_{33} + D^{H0}_{11}D^{H1}_{22}D^{H0}_{33} + D^{H0}_{11}D^{H0}_{22}D^{H1}_{33} + \cdots\right)\alpha \tag{A4}$$

which can be simplified as

$$|\mathbf{D}^{\mathbf{H}}| = (|D^{H}|)^{0} + (|D^{H}|)^{1}\alpha. \tag{A5}$$

Using a similar method, each component of c_{ij} can be obtained as

$$\begin{aligned} c_{11} &= \left(D^{H0}_{22} + D^{H1}_{22}\alpha\right)\left(D^{H0}_{33} + D^{H1}_{33}\alpha\right) - \left(D^{H0}_{32} + D^{H1}_{32}\alpha\right)\left(D^{H0}_{23} + D^{H1}_{23}\alpha\right) \\ &= \left(D^{H0}_{22}D^{H0}_{33} - D^{H0}_{32}D^{H0}_{23}\right) + \left(D^{H0}_{22}D^{H1}_{33} + D^{H1}_{22}D^{H0}_{33} - D^{H0}_{32}D^{H1}_{23} - D^{H1}_{32}D^{H0}_{23}\right)\alpha \end{aligned} \tag{A6}$$

$$\begin{aligned} c_{21} &= -\{(D_{12}^{H0}+D_{12}^{H1}\alpha)(D_{33}^{H0}+D_{33}^{H1}\alpha) \\ &\quad -(D_{32}^{H0}+D_{32}^{H1}\alpha)(D_{13}^{H0}+D_{13}^{H1}\alpha)\} \\ &= (D_{32}^{H0}D_{13}^{H0}-D_{12}^{H0}D_{33}^{H0}) \\ &\quad +(D_{32}^{H0}D_{13}^{H1}+D_{32}^{H1}D_{13}^{H0}-D_{12}^{H0}D_{33}^{H1}-D_{12}^{H1}D_{33}^{H0})\alpha \end{aligned} \tag{A7}$$

$$\begin{aligned} c_{31} &= -\{(D_{12}^{H0}+D_{12}^{H1}\alpha)(D_{23}^{H0}+D_{23}^{H1}\alpha) \\ &\quad -(D_{13}^{H0}+D_{13}^{H1}\alpha)(D_{22}^{H0}+D_{22}^{H1}\alpha)\} \\ &= (D_{13}^{H0}D_{22}^{H0}-D_{12}^{H0}D_{23}^{H0}) \\ &\quad +(D_{13}^{H0}D_{22}^{H1}+D_{13}^{H1}D_{22}^{H0}-D_{12}^{H0}D_{23}^{H1}-D_{12}^{H1}D_{23}^{H0})\alpha \end{aligned} \tag{A8}$$

$$\vdots$$

$$\mathbf{c}_{ij} = (c_{ij})^0 + (c_{ij})^1\alpha. \tag{A9}$$

Then, using the approximation of Equations (A4–A8), the stochastic compliance matrix $\mathbf{C}_{ij}^{\mathbf{H}}$ is written as

$$\mathbf{C}_{ij}^{\mathbf{H}} = \frac{(c_{ij})^0 + (c_{ij})^1\alpha}{(|D^H|)^0 + (|D^H|)^1\alpha}. \tag{A10}$$

Taking the approximation $1/(1+x) = 1 - x - x^2$, where $x \ll 1$, Equation (A10) can be written in an expanded form by neglecting the higher order of α.

$$\begin{aligned} \mathbf{C}_{ij}^{\mathbf{H}} &= \frac{(c_{ij})^0}{(|D^H|)^0} + \left(\frac{(c_{ij})^1(|D^H|)^0 - (c_{ij})^0(|D^H|)^1}{\left((|D^H|)^0\right)^2}\right)\alpha \\ &= (C_{ij}^H)^0 + (C_{ij}^H)^1\alpha. \end{aligned} \tag{A11}$$

Using a similar approach (for $i,j = (4,4),(5,5),(6,6)$) yields

$$\mathbf{C}_{ij}^{\mathbf{H}} = \frac{1}{\mathbf{D}_{ij}^{\mathbf{H}}} = \frac{1}{\left(D_{ij}^{H0}+D_{ij}^{H1}\alpha\right)} = \frac{1}{D_{ij}^{H0}} + \frac{D_{ij}^{H1}}{\left(D_{ij}^{H0}\right)^2}\alpha. \tag{A12}$$

A.2 The stochastically apparent elastic moduli

As the trabecular bone is an orthotropic material, the stochastic apparent elastic moduli are calculated as follow:

$$\mathbf{E}_{11}^{\mathbf{H}} = \frac{1}{C_{11}^{H0}} - \frac{C_{11}^{H1}}{(C_{11}^{H0})^2}\alpha = E_{11}^{H0} + E_{11}^{H1}\alpha, \tag{A13}$$

$$\mathbf{E}_{22}^{\mathbf{H}} = \frac{1}{C_{22}^{H0}} - \frac{C_{11}^{H1}}{(C_{22}^{H0})^2}\alpha = E_{22}^{H0} + E_{22}^{H1}\alpha, \tag{A14}$$

$$\mathbf{E}_{33}^{\mathbf{H}} = \frac{1}{C_{33}^{H0}} - \frac{C_{33}^{H1}}{\left(C_{33}^{H0}\right)^2}\alpha = E_{33}^{H0} + E_{33}^{H1}\alpha, \tag{A15}$$

$$\nu_{32}^{\mathbf{H}} = -\frac{E_{33}^{H0}}{C_{32}^{H0}} - \left(\frac{E_{33}^{H1}}{C_{32}^{H0}} + \frac{E_{33}^{H0}C_{32}^{H1}}{\left(C_{32}^{H0}\right)^2}\right)\alpha = \nu_{32}^{H0} + \nu_{32}^{H1}\alpha, \tag{A16}$$

$$\nu_{31}^{\mathbf{H}} = -\frac{E_{33}^{H0}}{C_{31}^{H0}} - \left(\frac{E_{33}^{H1}}{C_{31}^{H0}} + \frac{E_{33}^{H0}C_{31}^{H1}}{(C_{31}^{H0})^2}\right)\alpha = \nu_{31}^{H0} + \nu_{31}^{H1}\alpha, \tag{A17}$$

$$\nu_{21}^{\mathbf{H}} = -\frac{E_{22}^{H0}}{C_{21}^{H0}} - \left(\frac{E_{22}^{H1}}{C_{21}^{H0}} + \frac{E_{22}^{H0}C_{21}^{H1}}{(C_{21}^{H0})^2}\right)\alpha = \nu_{21}^{H0} + \nu_{21}^{H1}\alpha, \tag{A18}$$

$$\mathbf{G}_{23}^{\mathbf{H}} = \frac{1}{C_{44}^{H0}} - \frac{C_{44}^{H1}}{\left(C_{44}^{H0}\right)^2}\alpha = G_{23}^{H0} + G_{23}^{H1}\alpha, \tag{A19}$$

$$\mathbf{G}_{31}^{\mathbf{H}} = \frac{1}{C_{55}^{H0}} - \frac{C_{55}^{H1}}{\left(C_{55}^{H0}\right)^2}\alpha = G_{31}^{H0} + G_{31}^{H1}\alpha, \tag{A20}$$

$$\mathbf{G}_{12}^{\mathbf{H}} = \frac{1}{C_{66}^{H0}} - \frac{C_{66}^{H1}}{\left(C_{66}^{H0}\right)^2}\alpha = G_{12}^{H0} + G_{12}^{H1}\alpha. \tag{A21}$$

Finally, the expected value and variance of the apparent elastic moduli $\mathbf{S}^{\mathbf{H}}$ are calculated using the first-order perturbation's second moment as follows:

$$\mathrm{Exp}(\mathbf{S}^{\mathbf{H}}) = (S^H)^0, \tag{A22}$$

$$\mathrm{Var}(\mathbf{S}^{\mathbf{H}}) = (S^H)^1(S^H)^1\mathrm{cov}(\alpha,\alpha). \tag{A23}$$

Appendix B: Anisotropy set-up for trabecular bone tissue

As formulated in the main text, the compliance matrix $\mathbf{C}_{ij}$, considering the uncertainty of Young's modulus, can be written as follows:

$$\mathbf{C}_{ij}^{\mathbf{H}} = \begin{bmatrix} \frac{2}{E^0(1+\alpha)} & -\frac{\nu}{E^0(1+\alpha)} & -\frac{2\nu}{E^0(1+\alpha)} & 0 & 0 & 0 \\ -\frac{\nu}{E^0(1+\alpha)} & \frac{1}{E^0(1+\alpha)} & -\frac{\nu}{E^0(1+\alpha)} & 0 & 0 & 0 \\ -\frac{2\nu}{E^0(1+\alpha)} & -\frac{\nu}{E^0(1+\alpha)} & \frac{2}{E^0(1+\alpha)} & 0 & 0 & 0 \\ 0 & 0 & 0 & \frac{2(1+\nu)}{E^0(1+\alpha)} & 0 & 0 \\ 0 & 0 & 0 & 0 & \frac{2(1+\nu)}{E^0(1+\alpha)} & 0 \\ 0 & 0 & 0 & 0 & 0 & \frac{2(1+\nu)}{E^0(1+\alpha)} \end{bmatrix}. \tag{B1}$$

To obtain the stochastic bone tissue properties $\mathbf{D}_{ij}$, take the inverse of the compliance matrix.

$$\left(\mathbf{C}_{ij}^{\mathbf{H}}\right)^{-1} = \mathbf{D}_{ij}^{\mathbf{H}}. \tag{B2}$$

This manipulation yields

$$\mathbf{C}_{ij}^{\mathbf{H}} = \frac{E^0(1+\alpha)}{4} \times \begin{bmatrix} \frac{2-\nu^2}{(1-\nu-\nu^2)(\nu+1)} & \frac{2\nu}{(1-\nu-\nu^2)} & \frac{\nu^2+2\nu}{(1-\nu-\nu^2)(\nu+1)} & 0 & 0 & 0 \\ \frac{2\nu}{(1-\nu-\nu^2)} & \frac{4(1-\nu)}{(1-\nu-\nu^2)} & \frac{2\nu}{(1-\nu-\nu^2)} & 0 & 0 & 0 \\ \frac{\nu^2+2\nu}{(1-\nu-\nu^2)(\nu+1)} & \frac{2\nu}{(1-\nu-\nu^2)} & \frac{2-\nu^2}{(1-\nu-\nu^2)(\nu+1)} & 0 & 0 & 0 \\ 0 & 0 & 0 & \frac{4}{2(1+\nu)} & 0 & 0 \\ 0 & 0 & 0 & 0 & \frac{4}{2(1+\nu)} & 0 \\ 0 & 0 & 0 & 0 & 0 & \frac{4}{2(1+\nu)} \end{bmatrix}. \tag{B3}$$